

Article

Research on Path Tracking Fault-Tolerant Control Strategy for Intelligent Commercial Vehicles Based on Brake Actuator Failure

Guanjie Cui, Chunjiang Bao * , Mingjie Guo, Yahui Xu, Yelin He and Jian Wu 

School of Mechanical and Automotive Engineering, Liaocheng University, Liaocheng 252000, China; 2120230115@stu.lcu.edu.cn (G.C.); 2220230201@stu.lcu.edu.cn (M.G.); 2320230210@stu.lcu.edu.cn (Y.X.); 2320230204@stu.lcu.edu.cn (Y.H.); wujian@lcu.edu.cn (J.W.)

* Correspondence: baochunjiang@lcu.edu.cn

Abstract: With the development of safety technologies for intelligent commercial vehicles, electronic pneumatic braking systems (EBSs) have been widely used. However, EBS actuators may fail during vehicle operation and thus create safety problems. For this reason, we propose a path-tracking fault-tolerant control strategy under EBS actuator failure in intelligent commercial vehicles. First, in order to be able to characterize different types of brake actuator faults during the EBS differential braking process of a vehicle, a comprehensive fault coefficient for calculating the degree of fault is designed, and a BES generalized fault model is established. Second, the faults are introduced into the fault-tolerant controller through the comprehensive fault coefficients for braking torque calculation and braking pressure allocation. Thus, a vehicle path model with the complete fault coefficients as variable parameters is established. Then, based on the LPV system gain scheduling, a path-tracking LPV/ H_∞ fault-tolerant controller under EBS actuator faults in commercial vehicles is designed, which is used to solve the safety problem arising from sudden EBS actuator faults. Finally, we conducted experimental validation through hardware-in-the-loop tests. The results demonstrate that the control strategy designed in this paper redistributes the braking torque and synergizes with the steering system to enhance vehicle stability, thereby improving vehicle safety in the EBS failure mode.



Citation: Cui, G.; Bao, C.; Guo, M.; Xu, Y.; He, Y.; Wu, J. Research on Path Tracking Fault-Tolerant Control Strategy for Intelligent Commercial Vehicles Based on Brake Actuator Failure. *Actuators* **2024**, *13*, 97. <https://doi.org/10.3390/act13030097>

Academic Editor: Keigo Watanabe

Received: 26 January 2024

Revised: 20 February 2024

Accepted: 26 February 2024

Published: 28 February 2024



Copyright: © 2024 by the authors. Licensee MDPI, Basel, Switzerland. This article is an open access article distributed under the terms and conditions of the Creative Commons Attribution (CC BY) license (<https://creativecommons.org/licenses/by/4.0/>).

1. Introduction

Commercial vehicles play a crucial role in the global transportation industry, and their intelligence has a wide range of practical applications and commercial value [1]. As an important part of the chassis system of intelligent commercial vehicles, the braking system has been continuously developing in the direction of integration and modularization in recent years. The braking system can control the stability of the vehicle using differential braking, and differential braking has received widespread attention as a reliable solution for controlling the yaw stability of the vehicle [2–6]. The traditional pneumatic braking system has a long response time and low braking efficiency due to the delay of the air circuit system and the lag of the braking components, which can no longer meet the needs of people in terms of vehicle braking safety, comfort, and intelligence. The EBS combines traditional pneumatic braking with electronically controlled braking and attracts a lot of attention because of the advantages of precise braking force distribution and rapid response, which are widely used in intelligent commercial vehicles [7,8].

The increasing complexity of vehicle electromechanical structure functions also increases the possibility of system failure and malfunction, and it is challenging to realize redundancy for some critical components due to space and cost constraints. If the EBS actuator is damaged or malfunctions, it may result in decreased braking performance of the vehicle or may even make the vehicle less stable, increasing the risk of accidents [9]. Ensuring the stability and safety of a vehicle becomes a challenge when the actuator of the

EBS fails in an intelligent commercial vehicle. Based on the above analysis, we utilize the differential braking capability of EBS to design fault tolerance for actuator failure.

Fault-tolerant control is a control strategy that aims to minimize or prevent the impact of faults in highly reliable control systems. Its purpose is to ensure that a control system maintains stable operation and meets specific performance specifications in the event of a sensor, actuator, or meta-component failure. Fault-tolerant control currently has two development directions: active fault-tolerant control and passive fault-tolerant control [10,11]. In the field of vehicle fault-tolerant control, scholars have proposed a variety of active and passive fault-tolerant control strategies, including sliding mode control [12,13], adaptive control [14–16], fuzzy neural network control [17,18], and robust H_∞ and LPV control [19–22]. Passive fault-tolerant control is advantageous over active fault-tolerant control because it does not require fault detection and isolation units. So, it has the advantage of being easy to implement [23] and is more suitable for practical systems [24,25]. When sensors or actuators of a vehicle fail, fault-tolerant control is critical to ensure the vehicle's stability and safety [26–28].

In the case of actuator failure, a boundary layer-based sliding mode observer is devised for vehicle state estimates, while a delay estimation method is used for actuator failure estimation to assure that the vehicle retains its stability and path-tracking performance in the event of a failure [13]. Considering the problem of multiple actuator failures and dependence on accurate models during coordinated control of the driving and steering systems, a multi-input, multi-output model-less approach to model adaptive active fault-tolerant control has been proposed to address the complexity and nonlinearity of the vehicle models [15]. A fuzzy neural network-based active fault-tolerant control solution is able to monitor the speed problem of any wheel in real time to make sure that the state of vehicle stability is not affected when a wheel sensor or actuator failure occurs [18]. The aforementioned scholars presented a fault-tolerant control scheme for the problem of actuator failure, which effectively improves the validity of the system in the event of actuator faults, but it does not take into account the influence of perturbation on the control effect, and the robustness is low.

Based on the above analysis, the robustness of the controller needs to be further considered while taking into account the effect of actuator failure on the control effect. For damper faults as well as brake actuator faults, the three systems of steering, braking, and suspension are activated hierarchically and coordinated with each other by scheduling different parameters under the framework of the LPV system so as to improve vehicle comfort and stability [20]. For steering actuator faults, an LPV model for actuator faults containing velocity changes is developed, and the tracking and robust performance of the system is ensured by a robust control algorithm [21]. A fault-tolerant predictive controller is proposed for active suspension system sensor faults. To estimate the system state and sensor signal faults, a virtual observer is designed for the LPV system. The controller ensures stability and maintains control performance based on the observer information [22]. In the field of fault-tolerant control, LPV control and robust control can cope with internal parameter variations without changing the controller structure, which can better introduce fault modeling into the controller design and improve the robustness of the control system.

Currently, fault-tolerant control strategies of braking systems mainly realize error tolerance by redistributing the braking force and seldom consider the influence of the failure itself on the fault-tolerant controller, and the research objects are mainly focused on passenger cars, especially four-wheel independent drive electric vehicles [29–31], while relatively little research has been carried out on EBS for commercial vehicles. Therefore, we established a generalized fault model based on EBS to simulate the vast majority of faults that may occur in the actual operation of vehicles. A comprehensive fault coefficient was designed using the fault model based on which the state of the vehicle's EBS actuator was determined, and the braking force was assigned accordingly. Subsequently, the gain scheduling LPV robust H_∞ fault-tolerant controller under EBS actuator failure is designed.

This paper's primary contributions are as follows.

- (1) In an effort to better characterize various kinds of brake actuator faults during vehicle operation, this paper synthesizes a comprehensive fault coefficient on the basis of the ratio of actual brake pressure to ideal brake pressure so as to establish a generalized fault model of the EBS and introduce the comprehensive fault coefficient into the fault-tolerant controller design.
- (2) The influence of the brake actuator on the fault-tolerant controller design is fully considered, and a path-tracking LPV/ H_∞ fault-tolerant controller under EBS actuator faults in commercial vehicles is designed by using the robust H_∞ control framework and combining with the gain-scheduling LPV control algorithm, which is combined with the steering system in an effort to improve the stabilization and path-tracking properties of the vehicle.

The paper is structured as follows: Section 2 describes the vehicle and road model. Section 3 describes the brake actuator faults and models the faults. Section 4 designs the fault-tolerant controller according to the failure model. Section 5 conducts bench tests to derive the test results. Section 6 concludes.

2. Vehicle and Road Model

In this subsection, a dynamic model for lateral stabilization of a three-degree-of-freedom vehicle is first developed, considering only the transverse, lateral, and sideways tilting motions around the X-axis, as shown in Figure 1. Then, the model of path tracking control is given, as shown in Figure 2. Finally, the vertical load dynamics of the wheel are also modeled.

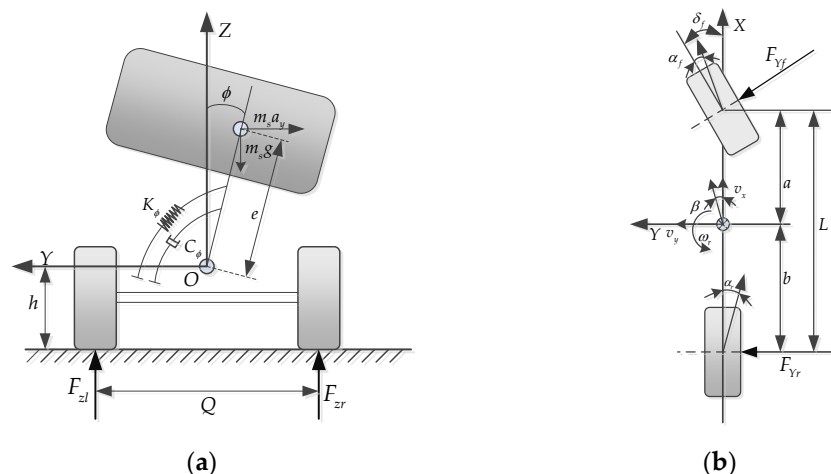


Figure 1. Intelligent bus three-degree-of-freedom traverse-sway coupling model. (a) Around the X-axis (b) Along the Y-axis and around the Z-axis.

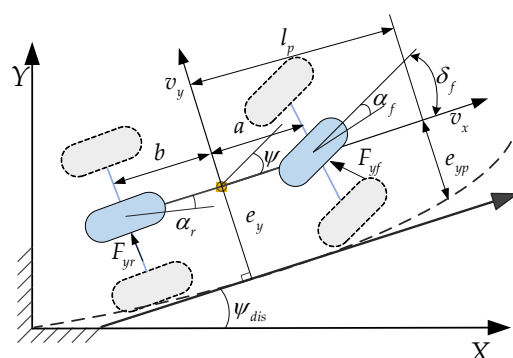


Figure 2. Path tracking control model, where ψ_{dis} is the expected heading angle; ψ is the actual heading angle; e_y is the lateral deviation of the vehicle's current position from the road centerline; e_{yp} is the lateral deviation at the pre-sighting point; l_p is the preview distance.

2.1. Vehicle Lateral Dynamics Model

Based on D'Alembert's principle, the equilibrium equations can be listed for the transverse motion along the Y-axis, the transverse pendulum motion around the Z-axis, and the lateral tilt motion around the X-axis [32]:

$$\begin{cases} \sum F_y = m(\omega_r v_x + \dot{v}_y) - m_s e \ddot{\phi} \\ \sum M_z = I_{zz} \dot{\omega}_r + I_{xz} \ddot{\phi} - M_z \\ \sum M_x = (I_{xx} + m_s e^2) \ddot{\phi} - m_s e (\omega_r v_x + \dot{v}_y) + I_{xz} \dot{\omega}_r \end{cases} \quad (1)$$

The sideslip angle $\beta = v_y/v_x$, then $\dot{\beta} = \dot{v}_y/v_x$; and the front and rear wheel side deflection angles are $\alpha_f = -\delta_f + \beta + a\omega_r/v_x$ and $\alpha_r = \beta - b\omega_r/v_x$, respectively, such that $I_{xs} = I_{xx} + m_s e^2$. Thus, (1) can be expressed as:

$$\begin{cases} \sum F_y = F_{Yf} + F_{Yr} = k_f \alpha_f + k_r \alpha_r \\ \sum M_z = aF_{Yf} - bF_{Yr} = ak_f \alpha_f - bk_r \alpha_r \\ \sum M_x = m_s g e \phi - K_\phi \phi - C_\phi \dot{\phi} \end{cases} \quad (2)$$

where the interpretation of the parameters used in the model is shown in Table 1.

Table 1. Model parameter interpretation.

Symbol	Description
m	Vehicle mass
m_s	Sprung mass
a	Distance from front axle to CG
b	Distance from rear axle to CG
I_{zz}	Yaw moment of inertia of sprung mass
I_{xx}	Roll moment of the inertia of sprung mass
I_{xz}	Yaw-roll product of inertia of sprung mass
k_f	Cornering stiffness of front tire
k_r	Cornering stiffness of rear tire
h	Centroid height
K_ϕ	Suspension roll stiffness
C_ϕ	Suspension roll damping
e	Height of CG of sprung mass from roll axis
ω_r	Yaw rate
ϕ	Sprung mass roll angle
v_y	Lateral velocity
M_z	Direct yaw moment
β	Side-slip angle at the center of mass

The matrix form of the motion differential equations of the three-degree-of-freedom vehicle model for intelligent commercial vehicles is described as:

$$\frac{d}{dt} x_1 = [H^{-1} J] x_1 + [H^{-1} F] u_1 \quad (3)$$

where state quantity $x_1 = [\beta \quad \omega_r \quad \phi \quad \dot{\phi}]^T$; control input $u_1 = [\delta_f \quad M_z]^T$,

$$H = \begin{bmatrix} mv_x & 0 & 0 & -m_s e \\ 0 & I_{zz} & 0 & I_{xz} \\ 0 & 0 & 1 & 0 \\ -m_s e v_x & I_{xz} & 0 & I_{xs} \end{bmatrix}, J = \begin{bmatrix} k_f + k_r & \frac{ak_f - bk_r}{v_x} - mv_x & 0 & 0 \\ ak_f - bk_r & \frac{a^2 k_f + b^2 k_r}{v_x} & 0 & 0 \\ 0 & 0 & 0 & 1 \\ 0 & m_s e v_x & m_s g e - K_\phi & -C_\phi \end{bmatrix},$$

$$F = \begin{bmatrix} k_f & 0 \\ ak_f & 1 \\ 0 & 0 \\ 0 & 0 \end{bmatrix}.$$

2.2. Path Tracking Control Model

In this paper, equations for the path tracking error due to vehicle motion and road trajectory changes are given [33].

$$\Delta\dot{\psi} = \omega_r - v_x\rho \quad (4)$$

$$\dot{e}_y = v_y \cos \Delta\psi + v_x \sin \Delta\psi \quad (5)$$

$$\dot{e}_{yp} = \dot{e}_y + v_x t_p \frac{d[\tan \Delta\psi]}{dt} \quad (6)$$

where $\Delta\psi$ is the angular deviation of the heading.

From Equations (4) and (5), we can get:

$$\dot{e}_{yp} = v_y \cos \Delta\psi + v_x \sin \Delta\psi + v_x t_p (\omega_r - v_x \rho) \quad (7)$$

where lateral velocity $v_y = \beta v_x$; consider $\Delta\psi$ as very small.

Then, Equation (7) can be written as:

$$\dot{e}_{yp} = v_x \beta + v_x \Delta\psi + v_x t_p \omega_r - v_x^2 t_p \rho \quad (8)$$

where t_p is the pre-sighting time, and ρ is the road curvature.

2.3. Vertical Load Dynamics Model of Wheel

The tire dynamic load was used to calculate the maximum value of braking torque for each tire, and for the load transfer during vehicle driving, the vertical load of each tire of the vehicle during driving is estimated as follows [34]:

$$\left\{ \begin{array}{l} F_{zlf} = \frac{mg}{2(a+b)} b - \frac{ma_x}{2(a+b)} h - \frac{m}{d(a+b)} bh(\dot{v}_y + v_x \omega_r) \\ F_{zlr} = \frac{mg}{2(a+b)} a + \frac{ma_x}{2(a+b)} h - \frac{m}{d(a+b)} bh(\dot{v}_y + v_x \omega_r) \\ F_{zrf} = \frac{mg}{2(a+b)} b - \frac{ma_x}{2(a+b)} h + \frac{m}{d(a+b)} bh(\dot{v}_y + v_x \omega_r) \\ F_{zrr} = \frac{mg}{2(a+b)} a + \frac{ma_x}{2(a+b)} h + \frac{m}{d(a+b)} bh(\dot{v}_y + v_x \omega_r) \end{array} \right. \quad (9)$$

where F_{zlf} , F_{zlr} , F_{zrf} , and F_{zrr} represent the vertical loads on the left front, left rear, right front, and right rear wheels of the vehicle, respectively; \dot{v}_y represents the lateral acceleration of the vehicle.

3. Brake Control System Fault Characterization

In this section, a broad fault model is established firstly for the possible faults of brake cylinder gas leakage and solenoid valve failure in the EBS system. Then, the broad failure model is combined with the EBS system to synthesize a comprehensive failure model.

The brake pressure and braking torque are related by the equation:

$$T_{bij} = \hat{\kappa}_{ij} P_{dij} = \kappa_{ij} \hat{P}_{mij} \quad (10)$$

where $i = \{l, r\}$ means left and right wheels; $j = \{f, r\}$ means front and rear wheels; T_{bij} means the target braking torque; P_{mij} means the sensor braking pressure; P_{dij} means the target braking pressure; $\hat{\kappa}_{ij}$ means the target braking pressure and target braking torque ratio coefficient for each brake wheel cylinder; κ_{ij} means the sensor braking pressure and target braking torque ratio coefficient for each brake wheel cylinder.

When $\hat{\kappa}_{ij}$ and κ_{ij} are not equal, it means that the target braking pressure does not match the sensor braking pressure, and the EBS has a malfunctioning component; the relationship is:

$$\hat{\kappa}_{ij} = \lambda_{ij} \kappa_{ij} = \frac{P_{mij}}{P_{dij}} \kappa_{ij} \quad (11)$$

Among others:

$$\lambda_{ij} = \frac{P_{mij}}{P_{dij}} \quad (12)$$

There may also be additional braking pressures generated by unknown factors during vehicle operation that make the true braking pressures:

$$\hat{P}_{mij} = P_{mij} + \Delta P_{ij} \quad (13)$$

where \hat{P}_{mij} is the true braking pressure; ΔP_{ij} is the additional braking pressure generated by unknown factors.

The above fault model can be formulated as (1) $\lambda_{ij} = 1$ and $\Delta P_{ij} = 0$, normal operation; (2) $\lambda_{ij} \in (0, 1)$, $\Delta P_{ij} \neq 0$, or $\Delta P_{ij} = 0$, failure fault; (3) $\lambda_{ij} = 1$ and $\Delta P_{ij} \neq 0$, additional fault; (4) $\lambda_{ij} = 0$, $\Delta P_{ij} \neq 0$, or $\Delta P_{ij} = 0$, brake holding fault.

Conventional vehicles generally realize direct transverse moment control by differential braking of the left and right wheels. When $|\omega_d| - |\omega_r| \geq 0$, understeer, the direct transverse moment of the target is generated by braking the inner wheel; when $|\omega_d| - |\omega_r| \leq 0$, oversteer, the direct transverse moment of the target is generated by braking the outer wheel.

The coefficient of brake torque distribution for front and rear wheels for a vehicle is:

$$\varepsilon = \frac{T_{blf}}{T_{blr}} = \frac{T_{brf}}{T_{brr}} \quad (14)$$

This gives a unilateral braking torque of:

$$T_i = \frac{\varepsilon \lambda_{if}}{1 + \varepsilon} T_{id} + \frac{\lambda_{ir}}{1 + \varepsilon} T_{id} \quad (15)$$

Set λ as the combined failure factor, the formula is as follows:

$$\lambda = \begin{cases} \frac{\lambda_{lr} + \lambda_{lf}\varepsilon}{1 + \varepsilon}, & \zeta \geq 0 \\ \frac{\lambda_{rr} + \lambda_{rf}\varepsilon}{1 + \varepsilon}, & \zeta < 0 \end{cases} \quad (16)$$

Formula in $0 < \lambda < 1$, $\zeta = \omega_r(|\omega_d| - |\omega_r|)$.

The EBS integrated fault model for direct transverse moment is as follows:

$$\begin{aligned} M_z &= \frac{Q}{2R_f} (T_i + \Delta T_l - \Delta T_r) \\ &= \lambda M_{zd} + \Delta M_z \end{aligned} \quad (17)$$

where Q is the front and rear axle wheelbase; R_t is the equivalent radius of the wheels; ΔT_l , ΔT_r are the additional braking moment of the left and right wheels, $\Delta T_l = \Delta T_{lf} + \Delta T_{lr}$, $\Delta T_r = \Delta T_{rf} + \Delta T_{rr}$; λ is the integrated failure coefficient; ΔM_z is the additional failure or external factors caused by the direct swing moment.

4. Fault-Tolerant Controller Design

In this section, an LPV/ H_∞ robust fault-tolerant controller is designed. Firstly, the LPV model is constructed, and the integrated fault coefficients in the previous section are used as time-varying parameters. Then, the LPV/ H_∞ controller is designed with state feedback, and the overall control scheme is shown in Figure 3.

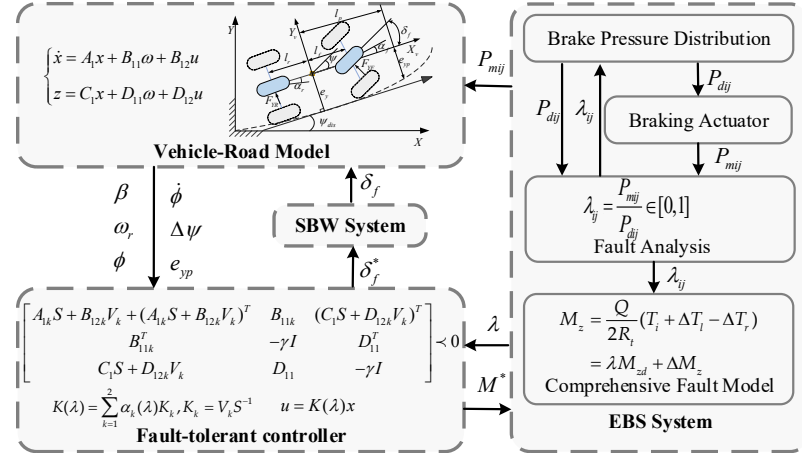


Figure 3. Fault-tolerant control scheme for lateral motion of intelligent commercial vehicles.

4.1. LPV Model

According to the linear parameter time-varying (LPV) control theory, the fault coefficients of each wheel proposed in this paper can be obtained in real time by calculating the actual wheel cylinder pressure and the desired wheel cylinder pressure. The fault coefficients can be obtained in real time by calculating the ratio between the target value and the actual value of the wheel cylinder pressure, and the integrated fault coefficients of the EBS can be synthesized in real time, which is in line with the design requirements of the LPV controller and ensures the effective control of the time-varying characteristics of the system.

According to the linear parameter time-varying (LPV) control theory, the fault coefficients λ_{ij} of each wheel proposed in this paper can be obtained by real-time calculation of the ratio of the actual value of the wheel cylinder pressure to the target value. The integrated fault coefficients λ of the EBS can be synthesized in real time from λ_{ij} , which meets the design requirements of the LPV controller and ensures the effective control of the system time-varying characteristics.

The system state equation of the vehicle–road closed-loop model is:

$$\frac{d}{dt}x = A_1x + B_{11}\omega + B_{12}u \quad (18)$$

Selection of state variables $x = [\beta \ \omega_r \ \phi \ \dot{\phi} \ e_{yp} \ \Delta\psi]^T$; control inputs $u = [\delta_f \ M_z]^T$; interference inputs $\omega = [\rho]$.

$$\text{Where } A_1 = \begin{bmatrix} H^{-1}J & 0 & 0 \\ v1 & 0 & v_x \\ v2 & 0 & 0 \end{bmatrix}, B_{11} = \begin{bmatrix} 0_{4 \times 1} \\ -v_x \\ -v_x^2 t_p \end{bmatrix}, B_{12} = \begin{bmatrix} H^{-1}F \\ 0 \\ 0 \end{bmatrix}, v1 = \begin{bmatrix} v_x \\ v_x t_p \\ 0 \\ 0 \end{bmatrix}^T, v2 = \begin{bmatrix} 0 \\ 1 \\ 0 \\ 0 \end{bmatrix}^T,$$

$$H = \begin{bmatrix} mv_x & 0 & 0 & -m_s e \\ 0 & I_{zz} & 0 & I_{xz} \\ 0 & 0 & 1 & 0 \\ -m_s e v_x & I_{xz} & 0 & I_{xs} \end{bmatrix}, J = \begin{bmatrix} k_f + k_r & \frac{ak_f - bk_r}{v_x} - mv_x & 0 & 0 \\ ak_f - bk_r & \frac{a^2 k_f + b^2 k_r}{v_x} & 0 & 0 \\ 0 & 0 & 0 & 1 \\ 0 & m_s e v_x & m_s g e - K_\phi & -C_\phi \end{bmatrix},$$

$$F = \begin{bmatrix} k_f & 0 \\ ak_f & 1 \\ 0 & 0 \\ 0 & 0 \end{bmatrix}.$$

The control objectives based on the robust control theory and this paper are mainly to ensure that the vehicle has a small road lateral position deviation, lateral inclination angle, and heading angle deviation during the traveling process. Define the auxiliary output vector $z = [\phi \quad \delta_f \quad M_z \quad e_{yp} \quad \Delta\psi]^T$.

$$z = C_1 x + D_{11} \omega + D_{12} u \quad (19)$$

$$\text{where } C_1 = \begin{bmatrix} 0 & 0 & q_1 & 0 & 0 & 0 \\ 0 & 0 & 0 & 0 & 0 & 0 \\ 0 & 0 & 0 & 0 & 0 & 0 \\ 0 & 0 & 0 & 0 & q_2 & 0 \\ 0 & 0 & 0 & 0 & 0 & q_3 \end{bmatrix}, D_{11} = \begin{bmatrix} 0 \\ 0 \\ 0 \\ 0 \\ 0 \end{bmatrix}, D_{12} = \begin{bmatrix} 0 & 0 \\ q_4 & 0 \\ 0 & q_5 \\ 0 & 0 \\ 0 & 0 \end{bmatrix}.$$

The vehicle-road LPV model is obtained as:

$$\begin{cases} \dot{x} = A_1 x + B_{11} \omega + B_{12} u \\ z = C_1 x + D_{11} \omega + D_{12} u \end{cases} \quad (20)$$

A linear matrix inequality (LMI)-based controller design method can be used for the quasi-LPV system described in Equation (20). The stability of the entire system is guaranteed by solving a set of linear matrix inequalities (LMIs) on the time-varying parameter trajectories [35]. However, due to the existence of an infinite number of LMIs on the time-varying parameter trajectory, in order to simplify the controller design process, the LPV system is transformed into a polytope formed by a convex composition of a limited number of vertices, and only the vertex controller is designed. This can greatly simplify the controller design and ensure system stability.

The multicellular form is a class of time-varying systems, and the system formula is expressed as:

$$\begin{cases} \dot{x} = A(\lambda) x + B(\lambda) u \\ z = C(\lambda) x + D(\lambda) u \end{cases} \quad (21)$$

The system matrix $S(\lambda) = \begin{bmatrix} A(\lambda) & B(\lambda) \\ C(\lambda) & D(\lambda) \end{bmatrix}$ takes the value of the given matrix polytope, i.e.,

$$S(\lambda) \in Co\{S_k, k = 1, \dots, r\} = \left\{ \sum_{k=1}^r \alpha_k S_k : 0 \leq \alpha_k \leq 1, \sum_{k=1}^r \alpha_k = 1 \right\} \quad (22)$$

where S_1, \dots, S_k is a known matrix; $S_1 = \begin{bmatrix} A_1 & B_1 \\ C_1 & D_1 \end{bmatrix}, \dots, S_k = \begin{bmatrix} A_k & B_k \\ C_k & D_k \end{bmatrix}$, whose corresponding convex combination coefficients are denoted as α_k .

α_k is the key to gain scheduling, and its calculation is shown by Figure 4 [36].

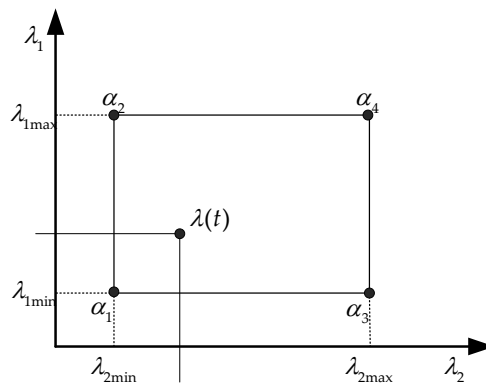


Figure 4. Polyhedral structure.

There is only one parameter variable in this article; therefore, the calculation formula for α_k is:

$$\alpha_1 = \frac{\lambda_{\max} - \lambda}{\lambda_{\max} - \lambda_{\min}}, \alpha_2 = \frac{\lambda - \lambda_{\min}}{\lambda_{\max} - \lambda_{\min}} \quad (23)$$

The multicellular form of the vehicle–road LPV model described by Equation (20) is:

$$\begin{bmatrix} A_1 & B_{11} & B_{12}(\lambda) \\ C_1 & D_{11} & D_{12} \end{bmatrix} = \sum_{k=1}^2 \alpha_k \begin{bmatrix} A_1 & B_{11} & B_{12k} \\ C_1 & D_{11} & D_{12} \end{bmatrix}, k = 1, 2 \quad (24)$$

4.2. State Feedback LPV/ H_∞ Controller Design

Based on the vehicle–road LPV model proposed in the previous section, a controller is devised such that the closed-loop system satisfies the following properties: (1) The control system exhibits parameter-dependent quadratic stability throughout the time-varying parameter ranges, i.e., the system is stable to parameter variations; (2) The transfer function of z from ω to a closed-loop system satisfies the H_∞ paradigm for a given requirement, i.e., the performance index should be less than an optimal value γ [37]. In addition, the controller is designed based on the LPV multi-cell type method and state-feedback H_∞ control theory in order to realize the above control objectives.

Let the form of the state feedback controller be:

$$u = K(\lambda)x \quad (25)$$

Such that $A_{cl} = A_1 + B_{12}(\lambda)K(\lambda)$ and $C_{cl} = C_1 + D_{12}K(\lambda)$. The Equation (20) can be expressed as follows:

$$\begin{cases} \dot{x} = A_{c1}(\lambda)x + B_{11}\omega \\ z = C_{c1}(\lambda)x + D_{11}\omega \end{cases} \quad (26)$$

The system (26) belongs to the linear parameter-dependent LPV systems with polytope structure, whose variable parameter scheduling factors depend on the state variable changes. By analyzing the stability of the vertices of the system polytope, it can be ensured that there is a linear relationship between the system parameters and the system matrix for the entire system. If the system is stable over the entire range of parameter variations, the vertices of the system polytope should be stable. Robust stability conditions are considered in the system to ensure that the system remains stable after a disturbance.

Lemma 1. (Bounded Real Theorem). *For a given continuous system (26) with transfer function $T_{z\omega}$, then the following conclusions are equivalent [37]:*

- (1) A_{c1} is stable, then there exists a robust performance indicator γ .

$$T_{z\omega} = \|G(s)\|_\infty = \left\|C_{c1}(SI - A_{c1})^{-1}B_{11} + D_{11}\right\|_\infty < \gamma \quad (27)$$

(2) A positive definite matrix P exists that satisfies the following linear matrix inequalities (LMIs):

$$T(K, P, \gamma) = \begin{bmatrix} A_{c1}^T P + PA_{c1} & PB_{11} & C_{c1}^T \\ B_{11}^T P & -\gamma I & D_{11} \\ C_{c1} & D_{11} & -\gamma I \end{bmatrix} < 0 \quad (28)$$

To ensure that the system has both dynamic and steady state properties, it is necessary to constrain the poles of the system to the appropriate region of the complex plane. In this paper, the analytical method of D–stability is used to analyze the stability of the multi-cellular vertices of the system.

Lemma 2. (D-stability). *To ensure the minimal attenuation rate α , minimal damper coefficient $\zeta = \cos\sigma$, and maximal intrinsic frequency $\omega_0 = rsin\sigma$ of the system, the closed-loop system's poles should be constrained to be within the area $S(\alpha, r, \sigma)$. There should exist a proper solution matrix P satisfying [38].*

$$\Omega_\Sigma^\alpha(K, P) = A_{c1}P + XP^T + 2\alpha P < 0 \quad (29)$$

$$\Omega_\Sigma^r(K, P) = \begin{bmatrix} -rP & A_{c1}P \\ PA_{c1}^T & -rP \end{bmatrix} < 0 \quad (30)$$

$$\Omega_\Sigma^\sigma(K, P) = \begin{bmatrix} (A_{c1}P + PA_{c1}^T) \sin\sigma & (A_{c1}P - PA_{c1}^T) \cos\sigma \\ (PA_{c1}^T - A_{c1}P) \cos\sigma & (PA_{c1}^T - A_{c1}P) \sin\sigma \end{bmatrix} < 0 \quad (31)$$

According to Equation (25), in conjunction with the question to be answered in this paper, the feedback control $K(\lambda)$ ensures both stability and robust stability of the system. Use the following theorem for the solution:

Theorem 1. *For each vertex of the multicellular form of the system (26), if there exists a feedback matrix K_k , matrix $P > 0$, and robust disturbance suppression criterion $\gamma > 0$, such as [37]*

$$T_{\Sigma(k)}(K_k, P, \gamma) < 0 \quad k = 1, 2 \quad (32)$$

$$\Omega_{\Sigma(k)}^\Xi(K_k, P) < 0 \quad k = 1, 2 \quad \Xi \in \{\alpha, r, \sigma\} \quad (33)$$

Then, the time-varying system (26) operating at any operating point λ satisfies

$$T_{\Sigma(k)}(K(\lambda), P, \gamma) = \sum_{k=1}^2 [\alpha_k(\lambda) T_{\Sigma(k)}(K_k, P, \gamma)] < 0 \quad (34)$$

$$\Omega_{\Sigma(k)}^\Xi(K(\lambda), P) = \sum_{k=1}^2 [\alpha_k(\lambda) \Omega_{\Sigma(k)}^\Xi(K_k, P)] < 0 \quad \Xi \in \{\alpha, r, \sigma\} \quad (35)$$

A linear matrix inequality is used according to Theorem 1 to solve for the positivity matrix P and the feedback gain matrix $K(\lambda)$. The following matrix inequality is obtained:

$$\begin{bmatrix} P(A_1 + B_{12}K) + (A_1 + B_{12}K)^T P & PB_{11} & (C_1 + D_{12}K)^T \\ B_{11}^T P & -\gamma I & D_{11}^T \\ C_1 + D_{12}K & D_{11} & -\gamma I \end{bmatrix} < 0 \quad (36)$$

The matrices are left-multiplied and right-multiplied, respectively, by $\text{diag}\{P^{-1}, I, I\}$.

$$\begin{bmatrix} A_1 P^{-1} + B_{12} K P^{-1} + P^{-1} A_1^T + P^{-1} K^T B_{12}^T & B_{11} & P^{-1} C_1^T + P^{-1} K^T D_{12}^T \\ B_{11}^T & -\gamma I & D_{11}^T \\ C_1 P^{-1} + D_{12} K P^{-1} & D_{11} & -\gamma I \end{bmatrix} < 0 \quad (37)$$

Let $S = P^{-1}$ and $V = KS$, then:

$$\begin{bmatrix} A_1 S + B_{12} V + (A_1 S + B_{12} V)^T & B_{11} & (C_1 S + D_{12} V)^T \\ B_{11}^T & -\gamma I & D_{11}^T \\ C_1 S + D_{12} V & D_{11} & -\gamma I \end{bmatrix} < 0 \quad (38)$$

That is, the following LMIs are finally solved:

$$\begin{bmatrix} A_1 S + B_{12k} V_k + (A_1 S + B_{12k} V_k)^T & B_{11} & (C_1 S + D_{12} V_k)^T \\ B_{11}^T & -\gamma I & D_{11}^T \\ C_1 S + D_{12} V_k & D_{11} & -\gamma I \end{bmatrix} < 0 \quad (39)$$

The feedback gain matrix for each vertex is K_k , then the feedback gain matrix is finally expressed as:

$$K(\lambda) = \sum_{k=1}^2 \alpha_k(\lambda) K_k, K_k = V_k S^{-1} \quad (40)$$

The feedback control strategy of the system is:

$$u = K(\lambda)x = \sum_{k=1}^2 \alpha_k(\lambda) K_k x \quad (41)$$

Figure 5 shows the pole distribution, where the symbol ‘★’ indicates the open-loop system poles at the apex of the parameter space, while ‘×’ indicates the closed-loop system poles near the apex of the parameter space. All the closed-loop system poles are confined limited to a specific sector $S(\alpha, r, \sigma)$, which guarantees the dynamic performance of the system.

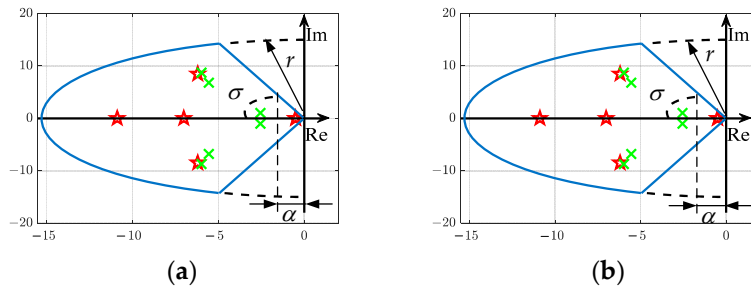


Figure 5. Distribution of open-loop and closed-loop poles. (a) $\lambda = 1$ (b) $\lambda = 0$.

4.3. Braking Torque Distribution

Brake force distribution is to realize the desired direct transverse moment of the upper control input through reasonable braking force distribution. According to wheel quasi-static dynamics, the relationship of wheel braking torque and longitudinal tire force is as follows [39]:

$$T_{bij} = R_t F_{xij} \quad (42)$$

where F_{xij} is the longitudinal tire force, N units.

Assuming that the vehicle mass distribution is symmetric, the direct transverse moment control quantity at the output of the upper controller is calculated as follows:

$$M_z = \frac{Q\Delta F_x}{2} \quad (43)$$

where ΔF_x is the difference between the longitudinal forces of the left and right wheels of the vehicle, in units of N. Then, the left and right wheel differential braking torque is calculated as follows:

$$\Delta T_b = T_{bl} - T_{br} = \frac{2M_z R_t}{Q} \quad (44)$$

where ΔT_b is the differential braking torque of the left and right wheels.

Considering the braking force saturation constraint of the road surface, combined with Equation (42), the maximum braking force that each wheel can provide is calculated as follows:

$$T_{bij} = T_{max} = \mu_f R_t F_{zij} \quad (45)$$

where T_{max} is the maximum braking torque that the road surface can provide; μ_f is the road surface adhesion coefficient.

The braking torque distribution algorithm proposed in this section is presented in Table 2:

Table 2. Logic table of braking torque distribution algorithm.

Front Wheel Angle	Yaw Rate	Yaw Rate Error	Vehicle Status	Brake Wheel
$\delta_f > 0$	$\omega_r > 0$	$\xi > 0$	Understeer	Left Wheel: $T_{blf}^* = (T_{blf}, T_{blfmax})$, $T_{blr}^* = (T_{blr}, T_{blrmax})$
		$\xi < 0$	Oversteer	Right Wheel: $T_{brf}^* = (T_{brf}, T_{brfmax})$, $T_{brr}^* = (T_{brr}, T_{brrmax})$
$\delta_f < 0$	$\omega_r < 0$	$\xi > 0$	Oversteer	Right Wheel: $T_{brf}^* = (T_{brf}, T_{brfmax})$, $T_{brr}^* = (T_{brr}, T_{brrmax})$
		$\xi < 0$	Understeer	Left Wheel: $T_{blf}^* = (T_{blf}, T_{blfmax})$, $T_{blr}^* = (T_{blr}, T_{blrmax})$

The steering wheel angle is positive when turning left; in the table: $\xi = |\omega_d| - |\omega_r|$, $T_{blf} = \frac{\lambda_{lf}}{\lambda_{lf} + \lambda_{lr}} \Delta T_b$, $T_{blr} = \frac{\lambda_{lr}}{\lambda_{lf} + \lambda_{lr}} \Delta T_b$, $T_{brf} = -\frac{\lambda_{rf}}{\lambda_{rf} + \lambda_{rr}} \Delta T_b$, $T_{brr} = -\frac{\lambda_{rr}}{\lambda_{rf} + \lambda_{rr}} \Delta T_b$.

5. Experimental Results and Analysis

In this section, the two experimental cases (S-turn and J-turn) are used to verify the performance of the fault-tolerant control strategy by utilizing TruckSim/Simulink and the HIL system. Two experimental cases, S-turn and J-turn, are designed for relatively sharp high-speed turning maneuvers. Different types of brake system faults were considered, including normal operation, additional faults, brake failure, and brake holding. The experiments assumed a uniform torque distribution between the front and rear wheels using the vehicle parameters listed in Table 3. The vehicle state parameter outputs are plotted for two cases to demonstrate the performance of the proposed fault-tolerant control strategy (LPV/ H_∞). The first case shows the LPV/ H_∞ controller's vehicle state parameter outputs without actuator faults, while the second case shows the LMI state feedback controller's vehicle state parameter outputs with actuator faults.

Table 3. Vehicle parameters.

Symbol	Value
m	10,690 kg
m_s	9360 kg
a	2.935 m
b	1.555 m
I_{zz}	30,782.4 kg·m ²
I_{xz}	4200 kg·m ²
I_{xx}	7695.6 kg·m ²
C_ϕ	82.56 KN·m·s/rad
Q	2.6 m
μ	0.85
k_f	-200 KN/rad
k_r	-350 KN/rad
K_ϕ	1104 KN·m/rad
e	0.67 m

5.1. Hardware-in-the-Loop System

Figure 6 shows the physical diagram of the commercial vehicle hardware-in-the-loop test platform used in this paper. It mainly consists of EBS, SBW system, upper computer, and lower computer.

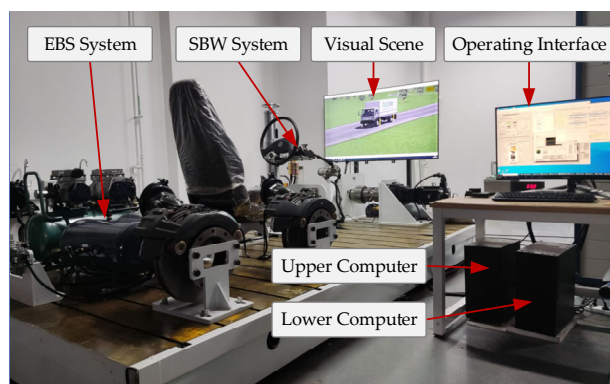


Figure 6. Commercial vehicle hardware-in-the-loop testbed.

Figure 7 illustrates the architecture of the implementation of a fault-tolerant control HIL system. The implementation process is as follows: first, the Simulink model written for the upper LPV controller and the vehicle dynamics model from TruckSim are embedded into the lower computer based on the NI PXI system. The lower computer executes the LPV controller algorithm in real time and sends the target corner to the underlying controller of the steering system. At the same time, the calculated direct swing torque determines the target pressure of the corresponding brake air chamber through the braking force distribution strategy and sends it to the lower controller. The underlying braking system calculates the opening and closing times of the solenoid valves using a PWM-like control method and controls the solenoid valves of the EBS to achieve the target braking pressure in the brake air chamber. After the steering system and brake system actuators generate actions, the corner sensor and brake chamber pressure sensor transmit the collected real values to the vehicle-road model of TruckSim in the lower computer via the CAN channel. TruckSim receives the control inputs and generates new state quantities, which are sent to the LPV controller in the lower computer to form a closed-loop control. At the same time, the analog quantities are converted to digital quantities by the DAQ data acquisition module of LabVIEW and displayed on the upper computer.

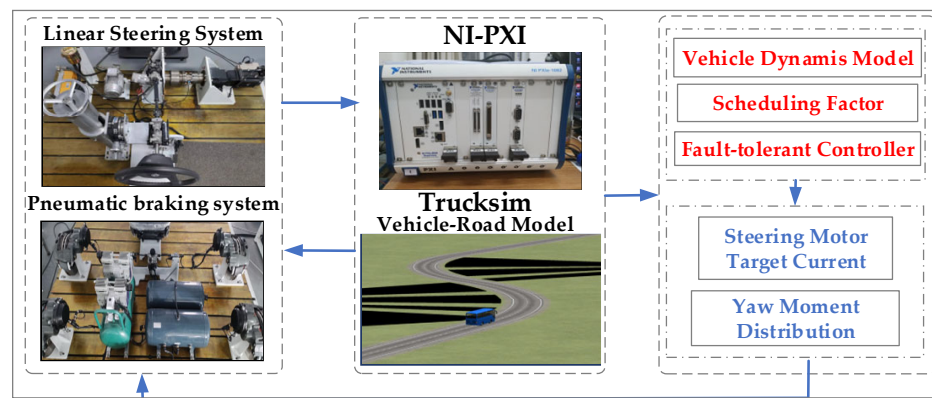


Figure 7. Fault-tolerant control HIL test framework for commercial vehicles.

5.2. Results and Analysis

Condition 1: S-turn condition. Vehicle speed $v = 60\text{km/h}$; road surface adhesion coefficient $\mu = 0.85$. EBS fault types include: at 3 s and 10 s, the left rear and right front wheels have brake failure faults, i.e., actual left rear wheel brake pressure is 0.4 times the target left rear wheel brake pressure $P_{mlr} = 0.4P_{dlr}$; actual right front wheel brake pressure is 0.4 times the target right front wheel brake pressure $P_{mrf} = 0.3P_{drf}$. The setting of brake actuator fault coefficients and comprehensive fault coefficients are shown in Figure 8.

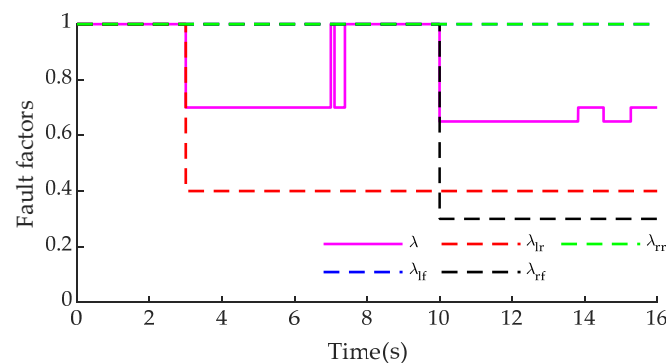


Figure 8. Failure coefficients of each brake wheel cylinder in the S-turn condition.

Figure 9 shows the experimental results when there is a partial failure fault of the brake actuator in the S-turn driving scenario. Figure 9a,b show outputs of the upper fault-tolerant controller, which is the steering wheel angle and direct yaw moment of the vehicle, respectively. When the brake actuator fails, the direct crossover torque control is reduced while the steering control is increased to compensate for the reduced direct yaw moment control. However, PID control does not work well in conjunction with the steering system to control vehicle stabilization. Figure 9c–e show the four-cylinder brake pressures, and when the left front and right rear wheels fail, their braking duties are reduced, thus decreasing the involvement of the failed actuator. Figure 9f shows the road curvature. Figure 9g,h show the variation of the vehicle's yaw rate and the sideslip angle. In the event of a fault, the fault-tolerant control strategy suggested in this paper keeps the vehicle's yaw rate and sideslip angle relatively stable. The maximum value of the vehicle's yaw rate does not exceed 0.2150 rad/s , and the maximum value of the sideslip angle does not exceed 1.1050° in all control strategies. This ensures the driving stability of the vehicle. Figure 9j illustrates the information about the trajectory tracking error. The fault-tolerant control strategy proposed can better ensure the trajectory tracking accuracy when the brake actuator failure fault occurs in this paper. The maximum values of trajectory tracking errors for the two fault-tolerant control strategies, except for PID control, are 0.0975 m and 0.1100 m , respectively. The PID control path error is relatively large and not very robust.

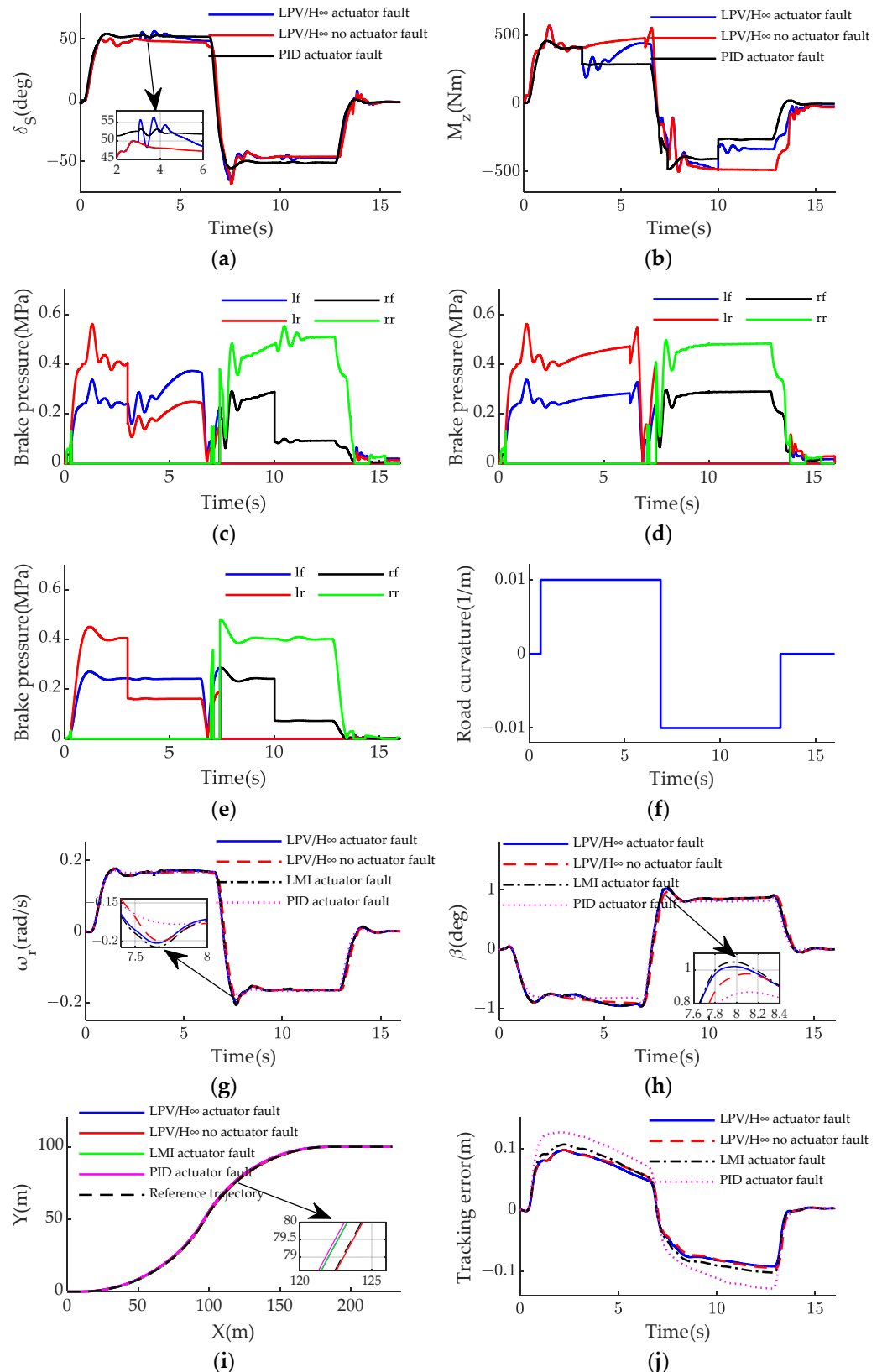


Figure 9. Plot of experimental results for S-turn conditions with failure fault types included. **(a)** Steering wheel angle **(b)** Direct yaw moment **(c)** LPV/ H_∞ actuator failure **(d)** LPV/ H_∞ without actuator failure **(e)** PID actuator failure **(f)** Road curvature **(g)** Yaw rate **(f)** Road curvature **(g)** Yaw rate **(h)** Sideslip angle **(i)** Vehicle trajectory **(j)** Trajectory tracking error.

In summary, under the S-turn condition, for the brake actuators with partial failure, the fault-tolerant control strategy proposed can optimize the braking performance of each brake actuator and the cooperative steering system and improve the safety and lateral stability of the vehicle driving process while ensuring high path tracking accuracy in this paper.

Condition 2: J-turn condition. Vehicle speed $v = 60\text{km/h}$; road surface adhesion coefficient $\mu = 0.85$. The EBS system fault types include: brake hold fault and extra fault for the left rear and left front wheels, respectively, at 3 s and 5 s, i.e., actual left rear wheel brake pressure is 0 times the target left rear wheel brake pressure $P_{mlr} = 0P_{dlr}$, $P_{mlf} = P_{dlf} + \Delta P_{lf}$ ($\Delta P_{lf} = 10\text{Nm}$). The setting of the brake actuator failure factor and the combined failure factor is shown in Figure 10.

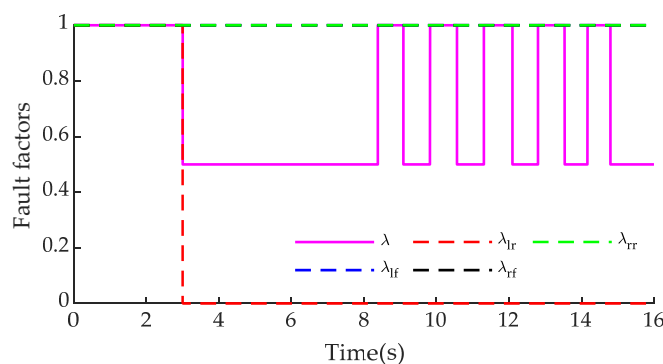


Figure 10. Failure coefficients of each brake wheel cylinder in the J-turn condition.

The validity of the fault-tolerant control strategy presented in coping with the stuck brake actuator fault and additional faults is verified by the experimental results shown in Figure 11 in the J-turn driving scenario in this paper. Figure 11a,b demonstrate the variation of steering wheel angle and direct yaw moment, indicating the synergistic effect of the fault-tolerant control strategy combined with a steering system. The PID control algorithm is insensitive to faults and basically does not react to the steering-braking control in the event of a fault. Figure 11c–e,g,h show that the pressure redistribution of the four brake wheel cylinders, as well as the stability of the vehicle's yaw rate and the sideslip angle, are also verified, with the maximum value of the vehicle's yaw rate not exceeding 0.2377 rad/s for all control strategies, and the maximum value of the vehicle's sideslip angle not exceeding 1.3567°. Figure 11f shows the road curvature. Figure 11i,j show that in terms of trajectory tracking, the fault-tolerant control strategy can reduce the maximum value of the trajectory tracking error, and the maximum values of the trajectory tracking error of the two fault-tolerant control strategies, except for PID control, are 0.1230 m and 0.1410 m, respectively. The PID control algorithm has a path-tracking error that becomes large when the path curvature increases and the risk of vehicle destabilization increases. It can be seen that the LPV/H ∞ control has higher robustness compared to the PID control algorithm. In summary, the fault-tolerant control strategy not only improves the stability of the vehicle's travel, safety, and accuracy of trajectory tracking but also strengthens the system's tolerance to the brake actuator failure in this paper.

In summary, under J-turn conditions, the fault-tolerant control strategy presented that includes the brake actuator fault factor in the brake force distribution combined with the steering system improves the safety and stability of the vehicle with good lateral path tracking effect to solve the brake actuator brake hold-up fault and other additional faults in this paper.

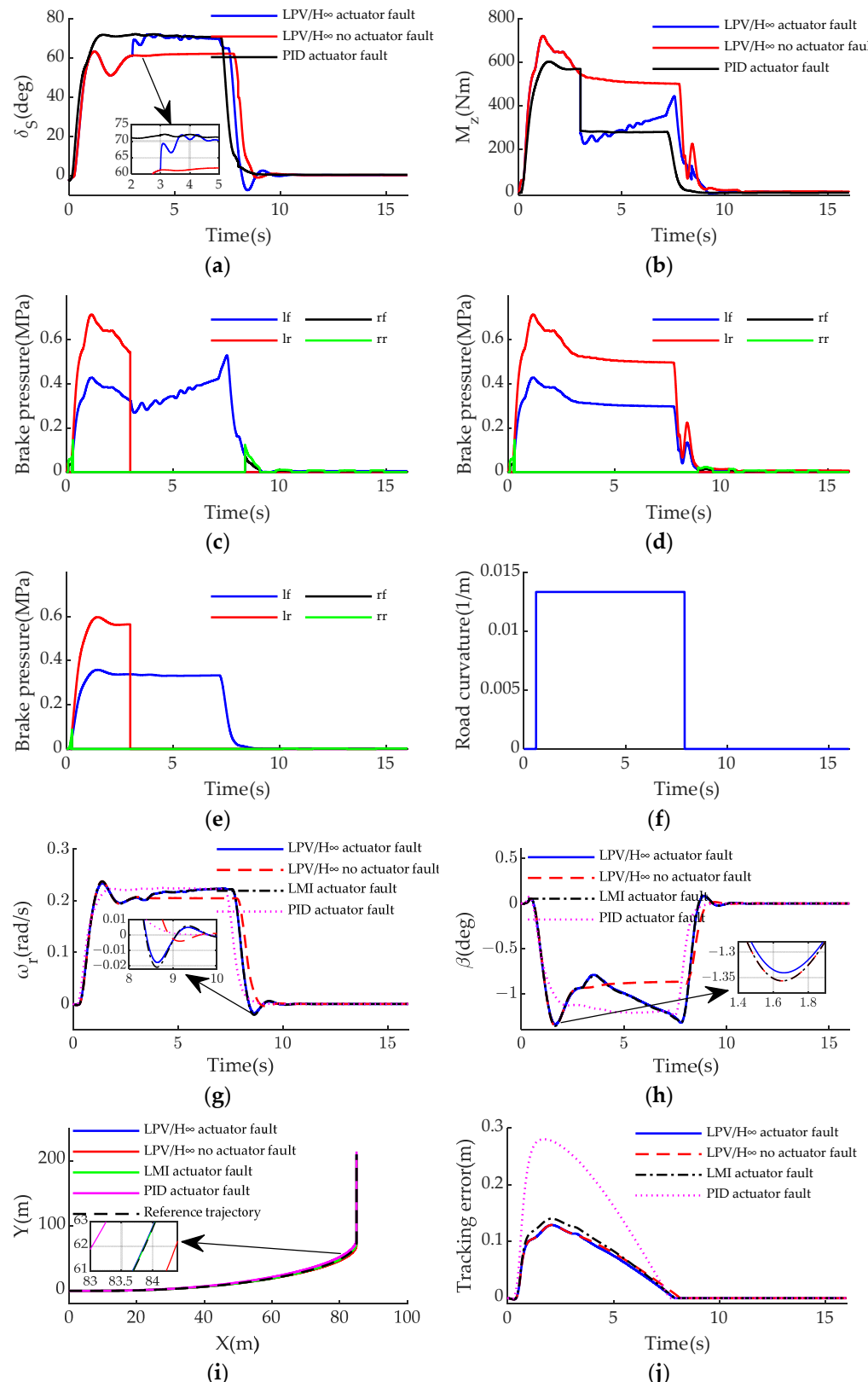


Figure 11. Plot of experimental results for the J-turn condition, including the type of stuck-at faults. **(a)** Steering wheel angle **(b)** Direct yaw moment **(c)** LPV/ H_∞ actuator failure **(d)** LPV/ H_∞ without actuator failure **(e)** PID actuator failure **(f)** Road curvature **(g)** Yaw rate **(h)** Sideslip angle **(i)** Vehicle trajectory **(j)** Trajectory tracking error.

6. Conclusions

In this paper, a novel state-feedback-based LPV/ H_∞ robust control method is proposed for improving the vehicle fault-tolerant control performance under EBS actuator faults in commercial vehicles. First, a generalized EBS fault model is constructed, and the comprehensive fault coefficients are designed based on the fault coefficients of each wheel to evaluate the EBS actuator state and assign the braking torque. Second, comprehensive fault coefficients are evaluated in real time to determine whether the EBS is faulty or not, and the gain scheduling LPV robust H_∞ fault-tolerant control strategy is adopted for realizing the fault-tolerant control of the EBS actuator fault. Finally, the control strategy designed in this paper is verified by a hardware-in-the-loop test, which proves that when the EBS actuator fails, the strategy can redistribute the braking torque and control it with the steering system in a cooperative manner to enhance the stability of the fault mode vehicle. It should be noted that only the effect of EBS actuator failure on the lateral stability of the vehicle is investigated in this paper, and the longitudinal dynamics also need to be considered in EBS control in this paper. Future research should add the effect of longitudinal dynamics on vehicle stability under EBS failure.

Author Contributions: Conceptualization, G.C. and C.B.; methodology, C.B. and G.C.; software, G.C.; validation, G.C., C.B., M.G., Y.X. and Y.H.; formal analysis, G.C. and M.G.; investigation, G.C.; resources, C.B.; data curation, G.C.; writing—original draft preparation, G.C.; writing—review and editing, C.B. and J.W.; visualization, G.C.; supervision, C.B. and J.W.; project administration, C.B.; funding acquisition, C.B. All authors have read and agreed to the published version of the manuscript.

Funding: This research was funded by the Key R&D Program of Shandong Province, China, grant number 2022CXPT025; Key R&D Program of Shandong Province, China, grant number 2023CXGC010214.

Data Availability Statement: The data presented in this study are available on request from the corresponding author.

Conflicts of Interest: The authors declare no conflicts of interest.

References

- Yan, Y.; Wu, J.; Liu, X.; Zhao, Y.; Wang, S. A lateral trajectory tracking control method for intelligent commercial vehicles considering active anti-roll decision based on Stackelberg equilibrium. *IET Intell. Transp. Syst.* **2022**, *16*, 1193–1208. [[CrossRef](#)]
- Zhang, B.; Zong, C.; Chen, G.; Huang, Y.; Xu, T. A novel integrated stability control based on differential braking and active steering for four-axle trucks. *Chin. J. Mech. Eng.* **2019**, *32*, 12. [[CrossRef](#)]
- Termous, H.; Shraim, H.; Talj, R.; Francis, C.; Charara, A. Coordinated control strategies for active steering, differential braking and active suspension for vehicle stability, handling and safety improvement. *Veh. Syst. Dyn.* **2018**, *57*, 1494–1529. [[CrossRef](#)]
- Mirzaeinejad, H.; Mirzaei, M.; Rafatnia, S. A novel technique for optimal integration of active steering and differential braking with estimation to improve vehicle directional stability. *ISA Trans.* **2018**, *80*, 513–527. [[CrossRef](#)] [[PubMed](#)]
- Abroshan, M.; Hajiloo, R.; Hashemi, E.; Khajepour, A. Model predictive-based tractor-trailer stabilisation using differential braking with experimental verification. *Veh. Syst. Dyn.* **2021**, *59*, 1190–1213. [[CrossRef](#)]
- Li, H.; Zheng, T.; Xia, F.; Gao, L.; Ye, Q.; Guo, Z. Emergency collision avoidance strategy for autonomous vehicles based on steering and differential braking. *Sci. Rep.* **2022**, *12*, 22647. [[CrossRef](#)]
- Karthikeyan, P.; Chaitanya, C.S.; Raju, N.J.; Subramanian, S.C. Modelling an electropneumatic brake system for commercial vehicles. *IET Electr. Syst. Transp.* **2011**, *1*, 41–48. [[CrossRef](#)]
- Zheng, H.; Ma, S.; Liu, Y. Vehicle braking force distribution with electronic pneumatic braking and hierarchical structure for commercial vehicle. *Proc. Inst. Mech. Eng. Part I J. Syst. Control. Eng.* **2018**, *232*, 481–493. [[CrossRef](#)]
- Kissai, M.; Mouton, X.; Monsuez, B. EPAS fail-safe control using differential braking. *Transp. Res. Procedia* **2021**, *52*, 300–306. [[CrossRef](#)]
- Jiang, J. Fault-tolerant control systems—an introductory overview. *Acta Autom. Sin.* **2005**, *31*, 161–174.
- Zhao, J.; Wang, X.; Liang, Z.; Li, W.; Wang, X.; Wong, P.K. Adaptive event-based robust passive fault tolerant control for nonlinear lateral stability of autonomous electric vehicles with asynchronous constraints. *ISA Trans.* **2022**, *127*, 310–323. [[CrossRef](#)]
- Ji, Y.; Zhang, J.; Liu, W.; Hou, X. *Fault-Tolerant Control of Regenerative Braking System on In-Wheel Motors Driven Electric Vehicles*; 0148-7191; SAE Technical Paper: Warrendale, PA, USA, 2020.
- Chen, T.; Chen, L.; Xu, X.; Cai, Y.; Jiang, H.; Sun, X. Passive actuator-fault-tolerant path following control of autonomous ground electric vehicle with in-wheel motors. *Adv. Eng. Softw.* **2019**, *134*, 22–30. [[CrossRef](#)]

14. Zhang, D.; Liu, G.; Zhou, H.; Zhao, W. Adaptive sliding mode fault-tolerant coordination control for four-wheel independently driven electric vehicles. *IEEE Trans. Ind. Electron.* **2018**, *65*, 9090–9100. [[CrossRef](#)]
15. Luo, Y.; Hu, Y.; Jiang, F.; Chen, R.; Wang, Y. Active fault-tolerant control based on multiple input multiple output-model free adaptive control for four wheel independently driven electric vehicle drive system. *Appl. Sci.* **2019**, *9*, 276. [[CrossRef](#)]
16. Lu, Y.; Xu, X.; Qiao, L.; Zhang, W. Robust adaptive formation tracking of autonomous surface vehicles with guaranteed performance and actuator faults. *Ocean Eng.* **2021**, *237*, 109592. [[CrossRef](#)]
17. Zhang, G.; Chu, S.; Jin, X.; Zhang, W. Composite neural learning fault-tolerant control for underactuated vehicles with event-triggered input. *IEEE Trans. Cybern.* **2020**, *51*, 2327–2338. [[CrossRef](#)]
18. Alsuwian, T.; Usman, M.H.; Amin, A.A. An Autonomous Vehicle Stability Control Using Active Fault-Tolerant Control Based on a Fuzzy Neural Network. *Electronics* **2022**, *11*, 3165. [[CrossRef](#)]
19. Gáspár, P.; Szabó, Z.; Bokor, J. LPV design of fault-tolerant control for road vehicles. In Proceedings of the 2010 Conference on Control and Fault-Tolerant Systems (SysTol), Nice, France, 6–8 October 2010; pp. 807–812.
20. Fergani, S.; Senane, O.; Dugard, L.; Gáspár, P. Further development on the LPV fault tolerant control for vehicle dynamics. *IFAC-PapersOnLine* **2015**, *48*, 24–29. [[CrossRef](#)]
21. Chen, M.; Ren, Y.; Ou, M. Robust path following control for autonomous vehicle considering actuator fault. In *Proceedings of the Big Data and Internet of Things School, Chongqing Vocational Institute of Engineering, Chongqing, China, 12–14 August 2022*; College of Engineering and Technology, Southwest University: Chongqing, China, 2022; p. 012033.
22. Abboudi, A.; Bououden, S.; Chadli, M.; Boulkaibet, I.; Neji, B. Observer-based fault-tolerant predictive control for LPV systems with sensor faults: An active car suspension application. *Appl. Sci.* **2022**, *12*, 684. [[CrossRef](#)]
23. Cao, X.; Tian, Y.; Ji, X.; Qiu, B. Fault-tolerant controller design for path following of the autonomous vehicle under the faults in braking actuators. *IEEE Trans. Transp. Electrif.* **2021**, *7*, 2530–2540. [[CrossRef](#)]
24. Djaziri, M.A.; Merzouki, R.; Bouamama, B.O.; Ouladsine, M. Fault diagnosis and fault-tolerant control of an electric vehicle overactuated. *IEEE Trans. Veh. Technol.* **2012**, *62*, 986–994. [[CrossRef](#)]
25. Hu, C.; Wei, X.; Ren, Y. Passive fault-tolerant control based on weighted LPV tube-MPC for air-breathing hypersonic vehicles. *Int. J. Control Autom. Syst.* **2019**, *17*, 1957–1970. [[CrossRef](#)]
26. Mahmoud, M.S.; Xia, Y. *Analysis and Synthesis of Fault-Tolerant Control Systems*; John Wiley & Sons: Hoboken, NJ, USA, 2013.
27. Ou, J.; Yan, D.; Zhang, Y.; Yang, E.; Huang, D. Research on the Stability Control Strategy of Distributed Electric Vehicles Based on Cooperative Reconfiguration Allocation. *World Electr. Veh. J.* **2023**, *14*, 31. [[CrossRef](#)]
28. Yan, M.; Chen, W.; Wang, Q.; Zhao, L.; Cai, B.; Liu, S. Fault-tolerant human-machine shared scheme for collision avoidance of intelligent vehicles considering driver error and actuator fault. *Veh. Syst. Dyn.* **2023**, *61*, 2912–2935. [[CrossRef](#)]
29. Huang, X.; Zha, Y.; Lv, X.; Quan, X. Torque Fault-Tolerant Hierarchical Control of 4WID Electric Vehicles Based on Improved MPC and SMC. *IEEE Access* **2023**, *11*, 132718–132734. [[CrossRef](#)]
30. Stolte, T.; Loba, M.; Nee, M.; Wu, L.; Maurer, M. Toward Fault-Tolerant Vehicle Motion Control for Over-Actuated Automated Vehicles: A Non-Linear Model Predictive Approach. *IEEE Access* **2023**, *11*, 10499–10519. [[CrossRef](#)]
31. Lee, K.; Lee, M. Fault-tolerant stability control for independent four-wheel drive electric vehicle under actuator fault conditions. *IEEE Access* **2020**, *8*, 91368–91378. [[CrossRef](#)]
32. Vu, V.T.; Senane, O.; Dugard, L.; Gáspár, P. Enhancing roll stability of heavy vehicle by LQR active anti-roll bar control using electronic servo-valve hydraulic actuators. *Veh. Syst. Dyn.* **2017**, *55*, 1405–1429. [[CrossRef](#)]
33. Yang, K.; Liu, Y.; Na, X.; He, X.; Liu, Y.; Wu, J.; Nakano, S.; Ji, X. Preview-scheduled steering assistance control for co-piloting vehicle: A human-like methodology. *Veh. Syst. Dyn.* **2019**, *58*, 518–544. [[CrossRef](#)]
34. Zhai, L.; Sun, T.; Wang, J. Electronic stability control based on motor driving and braking torque distribution for a four in-wheel motor drive electric vehicle. *IEEE Trans. Veh. Technol.* **2016**, *65*, 4726–4739. [[CrossRef](#)]
35. Wu, J.; Kong, Q.; Yang, K.; Liu, Y.; Cao, D.; Li, Z. Research on the steering torque control for intelligent vehicles co-driving with the penalty factor of human-machine intervention. *IEEE Trans. Syst. Man Cybern. Syst.* **2022**, *53*, 59–70. [[CrossRef](#)]
36. Zhang, H.; Zhang, X.; Wang, J. Robust gain-scheduling energy-to-peak control of vehicle lateral dynamics stabilisation. *Veh. Syst. Dyn.* **2014**, *52*, 309–340. [[CrossRef](#)]
37. Apkarian, P.; Gahinet, P.; Becker, G. Self-scheduled H_∞ control of linear parameter-varying systems: A design example. *Automatica* **1995**, *31*, 1251–1261. [[CrossRef](#)]
38. Toulouze, P.-F.; Delprat, S.; Guerra, T.-M.; Boonaert, J. Vehicle spacing control using robust fuzzy control with pole placement in LMI region. *Eng. Appl. Artif. Intell.* **2008**, *21*, 756–768. [[CrossRef](#)]
39. Fergani, S.; Senane, O.; Dugard, L. A LPV/ H_∞ Global Chassis Controller for performances Improvement Involving Braking, Suspension and Steering Systems. *IFAC Proc. Vol.* **2012**, *45*, 363–368. [[CrossRef](#)]

Disclaimer/Publisher’s Note: The statements, opinions and data contained in all publications are solely those of the individual author(s) and contributor(s) and not of MDPI and/or the editor(s). MDPI and/or the editor(s) disclaim responsibility for any injury to people or property resulting from any ideas, methods, instructions or products referred to in the content.